




# Suppression of neuronal CDK9/p53/VDAC signaling provides bioenergetic support and improves post-stroke neuropsychiatric outcomes

Jing Xia<sup>1,2</sup> · Tingting Zhang<sup>1,2,3</sup> · Ying Sun<sup>1,2</sup> · Zhu Huang<sup>1,2</sup> · Dingfang Shi<sup>1,2</sup> · Dongshen Qin<sup>1,2</sup> · Xuejun Yang<sup>1,2</sup> · Hao Liu<sup>1,2,3</sup> · Guiying Yao<sup>3</sup> · Libin Wei<sup>1</sup> · Xiaoi Chang<sup>4</sup> · Jun Gao<sup>4</sup> · Yongjian Guo<sup>1,5</sup> · Xiao-Yu Hou<sup>1,2</sup> 

Received: 21 May 2024 / Revised: 30 July 2024 / Accepted: 27 August 2024  
© The Author(s) 2024

## Abstract

Bioenergy decline occurs with reperfusion following acute ischemic stroke. However, the molecular mechanisms that limit energy metabolism and their impact on post-stroke cognitive and emotional complications are still unclear. In the present study, we demonstrate that the p53 transcriptional response is responsible for neuronal adenosine triphosphate (ATP) deficiency and progressively neuropsychiatric disturbances, involving the downregulation of mitochondrial voltage-dependent anion channels (VDACs). Neuronal p53 transactivated the promoter of *microRNA-183* (*miR-183*) cluster, thereby upregulating biogenesis of *miR-183-5p* (*miR-183*), *miR-96-5p* (*miR-96*), and *miR-182-5p*. Both *miR-183* and *miR-96* directly targeted and post-transcriptionally suppressed VDACs. Neuronal ablation of p53 protected against ATP deficiency and neurological deficits, whereas post-stroke rescue of *miR-183*/VDAC signaling reversed these benefits. Interestingly, cyclin-dependent kinase 9 (CDK9) was found to be enriched in cortical neurons and upregulated the p53-induced transcription of the *miR-183* cluster in neurons after ischemia. Post-treatment with the CDK9 inhibitor oroxylin A promoted neuronal ATP production mainly through suppressing the *miR-183* cluster/VDAC axis, further improved long-term sensorimotor abilities and spatial memory, and alleviated depressive-like behaviors in mice following stroke. Our findings reveal an intrinsic CDK9/p53/VDAC pathway that drives neuronal bioenergy decline and underlies post-stroke cognitive impairment and depression, thus highlighting the therapeutic potential of oroxylin A for better outcomes.

**Keywords** Cerebral ischemia · Glucose metabolism · Mitochondrial transporter · Neuronal energy metabolism · Post-stroke cognitive impairment · Post-stroke depression

## Abbreviations

AIS	Acute ischemic stroke	CDK9	Cyclin-dependent kinase 9
ATP	Adenosine triphosphate	COX4	Cytochrome c oxidase subunit 4
CBF	Cerebral blood flow	DLR	Dual-luciferase reporter
		DMEM	Dulbecco's modified Eagle's medium

Jing Xia, Tingting Zhang and Ying Sun contributed equally to this work.

✉ Jun Gao  
gaojun@njmu.edu.cn

✉ Yongjian Guo  
guoyj@cpu.edu.cn

✉ Xiao-Yu Hou  
xyhou@cpu.edu.cn

<sup>1</sup> State Key Laboratory of Natural Medicines, China Pharmaceutical University, Nanjing, Jiangsu 211198, China

<sup>2</sup> School of Life Science and Technology, China Pharmaceutical University, Nanjing, Jiangsu 211198, China

<sup>3</sup> Research Center for Biochemistry and Molecular Biology, Xuzhou Medical University, Xuzhou, Jiangsu 221004, China

<sup>4</sup> School of Basic Medical Sciences, Nanjing Medical University, Nanjing, Jiangsu 211166, China

<sup>5</sup> School of Biopharmacy, China Pharmaceutical University, Nanjing, Jiangsu 211198, China

G6PD	Glucose-6-phosphate dehydrogenase
HK1	Hexokinase 1
I/R	Ischemia-reperfusion
IF	Immunofluorescence
LDHA	Lactate dehydrogenase A
<i>miR</i>	MicroRNA
mNSS	Modified neurological severity score
MUT	Mutated form
NC	Negative control
OGD	Oxygen and glucose deprivation
PFK1	Phosphofructokinase 1
PFT- $\alpha$	Pifithrin- $\alpha$
PFT- $\mu$	Pifithrin- $\mu$
PREs	Putative response elements
PSCI	Post-stroke cognitive impairment
PSD	Post-stroke depression
qPCR	Quantitative polymerase chain reaction
tMCAO	Transient middle cerebral artery occlusion
<i>TP53</i>	Tumor protein 53 gene
<i>Trp53</i>	Transformation-related protein 53 gene
TTC	2, 3, 5-triphenyltetrazolium chloride
UPR	Upstream promoter region
UTR	Untranslated region
VDAC	Mitochondrial voltage-dependent anion channel
WT	Wild type

## Introduction

Acute ischemic stroke (AIS) is a major cause of adult disability and mortality, and its incidence is increasing among adults, including young and middle-aged adults [1, 2]. Early re-establishment of cerebral blood flow (CBF) and widely performed clinical interventions for AIS using intravenous thrombolysis and endovascular mechanical thrombectomy lead to a reduction in disability and mortality [3, 4]. However, cerebral ischemia-reperfusion (I/R) is often concomitant with progressive cerebral infarction, leading to poor sensorimotor outcomes. Long-term post-stroke cognitive impairment (PSCI) and post-stroke depression (PSD) frequently occur in stroke survivors; however, the underlying cellular and molecular mechanisms remain elusive [5–7]. Few effective therapeutic drugs have been approved for the prevention of PSCI and PSD.

The mammalian brain is highly dependent on bioenergy supply relative to other organs because neurons require energy for axonal transport, synaptic transmission, and cognition [8–10]. Transient cerebral ischemia induces almost complete adenosine triphosphate (ATP) depletion, and bioenergetic metabolism recovers transiently with the onset of CBF reintroduction, which is followed by a sustained decline in ATP levels [11, 12]. Bioenergy deficiency

induces neuronal cell death [12, 13] and affects neural network remodeling after cerebral ischemia [14], which may progressively aggravate cerebral infarction and neurocognitive deficits. However, the development of PSD is not correlated with lesion volume in stroke survivors [15]. Interestingly, brain metabolic decline and network disintegration in patients are involved in the development of treatment-resistant major depression disorder [16, 17]. Therefore, we speculate that bioenergy decline underlies neurocognitive dysfunction and emotional status after stroke. However, the key molecular pathways that drive post-stroke metabolic dysregulation are largely unknown.

The transcription factor p53, a well-known tumor suppressor, is encoded by the human tumor protein 53 (*TP53*) gene that is orthologous to the mouse transformation-related protein 53 (*Trp53*) gene. In the mammalian brain, p53 is expressed throughout perinatal development and maintained thereafter at relatively low levels through ubiquitin-proteasomal degradation. Human *TP53* polymorphism is associated with the clinical consequences of stroke, including lesion volume and motor disability [18, 19]. The transcriptional activity of p53 induces *C9orf72*poly(PR)-related neurodegenerative disorder [20]. After ischemic stroke, p53 accumulates in cortical neurons and contributes to neuronal apoptosis through transcription-dependent and -independent pathways [21]. Although the functional significance of p53 in post-stroke brain damage has been previously explored, pharmacological interventions that directly target p53 for brain disease treatment involve the risk of tumorigenicity. In various cancer cells, p53 transcriptionally regulates cell cycle arrest, apoptosis, and senescence and thereby limits tumor progression by its target gene products [22–24]. In response to DNA damage, p53 induces the mitochondrial apoptosis pathway through its transcription-independent function [25]. Transcription-independent functions also direct p53 to select the appropriate DNA damage repair pathway to maintain genomic stability, thus suppressing tumorigenesis [26, 27]. Although p53-regulated responses act as central events in cancer pathology, little is known about the upstream regulators of p53 and downstream cellular and molecular events in the context of neurological disorders.

In this study, we investigated the link between intrinsic p53 signaling pathways and bioenergy failure in neurons of peri-infarct tissue and its contribution to PSCI and PSD. Our results showed that neuronal p53 transcriptional activity disrupts the energy metabolic process through the *microRNA-183* (*miR-183*) cluster/mitochondrial voltage-dependent anion channel (VDAC) axis. We also investigated the cellular distribution of cyclin-dependent kinase 9 (CDK9) and its regulatory role in p53 transcriptional signaling events, and further explored the therapeutic significance

of the small-molecule CDK9 inhibitor oroxylin A in long-term sensorimotor and neuropsychiatric disturbances after AIS. Our data revealed that the CDK9/*miR-183* cluster signaling cascade represents a potential druggable target for improving long-term post-stroke neuropsychiatric outcomes.

## Materials and methods

### Experimental animals

Adult male and female C57BL/6 mice were purchased from Cavens Laboratory Animal (Changzhou, Jiangsu, China) and SIPPR-BK Lab Animal Ltd. (Shanghai, China). *Trp53*<sup>+/-</sup> heterozygous mice were purchased from Biocytogen Pharmaceuticals (Beijing, China), and *Trp53*-floxed (*Trp53*<sup>flox/flox</sup>) mice were purchased from Jackson Laboratory (Marine, USA). The animals were housed under a 12-h light/dark cycle and provided *ad-libitum* access to food and water. All animals were randomly assigned to experimental groups, and all procedures followed the guidelines of the National Science and Technology Commission and were approved by the Institutional Animal Care and Use Committee of China Pharmaceutical University.

### Transient middle cerebral artery occlusion (tMCAO) model and drug treatment

Adult C57BL/6 mice (25 ± 3 g, 10–12 weeks old) were anesthetized with isoflurane, and right MCA occlusion was induced with a silicon-coated monofilament suture [12]. Reperfusion was achieved by withdrawing the sutures after 60 min of occlusion. CBF change was monitored using a CBF imager (FLPI-2, Gene & I, Beijing, China). Pifithrin- $\alpha$  (PFT- $\alpha$ ) or pifithrin- $\mu$  (PFT- $\mu$ ) was administered to specifically inhibit p53 transcription-dependent or -independent activity, respectively. PFT- $\alpha$  (Selleck, S2929, Texas, USA) and PFT- $\mu$  (Selleck, S2930) were intraperitoneally injected half an hour before tMCAO. For conditional knockout of p53 in cortical neurons or astrocytes, AAV-CaMKII $\alpha$ -Cre or AAV-GFAP-Cre (1 × 10<sup>9</sup> viral; Obio Technology, Shanghai, China) or their negative controls (NC) were injected into the cerebral cortex (ML, ± 3.0 mm; DV, -2.2 mm) of *Trp53*<sup>flox/flox</sup> mice two to three weeks prior to tMCAO. We injected *miR-183* mimics (300 pmol) and *miR-NC* (GenePharma, Shanghai, China) into the lateral ventricle (AP, -0.2 mm from bregma; ML, -1.0 mm; DV, -2.5 mm) within 50 min after tMCAO. Oroxylin A (kindly provided by Prof. Zhiyu Li at China Pharmaceutical University) was intravenously injected 30 min after tMCAO.

### Cell culture and oxygen and glucose deprivation (OGD)

Mouse hippocampal HT22 neuronal cells and HEK293 cells were cultured in complete medium (Dulbecco's modified Eagle's medium [DMEM; Gibco, 12800-058, PA, USA] supplemented with 10% fetal bovine serum [ExCell Bio, FSP500, Shanghai, China]) at 37 °C under normoxic conditions (5% CO<sub>2</sub>, 95% air). For OGD treatment, HT22 cells were cultured in glucose-free DMEM (Pricella, PM150270, Wuhan, China) after 12 h of transfection with luciferase reporter plasmids pGL3-basic-PRE (wild type [WT]) or pGL3-basic-PRE (mutated [MUT]), and then placed into a hypoxic chamber (Thermo Fisher Scientific, PA, USA) with 1% O<sub>2</sub>, 94% N<sub>2</sub>, and 5% CO<sub>2</sub> for 3 h. Cells were allowed to recover (OGD/R) in complete culture medium under normoxic conditions. HT22 cells incubated with glucose-free DMEM under normoxic conditions served as the control. The cells were collected for luciferase activity assays.

### Immunoblot

Peri-infarct tissue samples were collected from mouse brains 24 h after reperfusion and homogenized in ice-cold buffer [12] containing protease inhibitors (Beyotime, P1005, Beijing, China). The protein concentration was measured using the Lowry method. Proteins were separated using sodium dodecyl sulfate-polyacrylamide gel electrophoresis and transferred onto nitrocellulose membranes. The membranes were blocked with 3% bovine serum albumin for 1 h, incubated with specific primary antibodies, and then horseradish peroxidase-conjugated secondary antibodies (listed in Supplementary Table S1). The blots were visualized using a Chemiluminescence Detection Kit (Vazyme, E412, Nanjing, China) and the Amersham ImageQuant800 system (Cytiva, Marlborough, USA), and the resulting bands were analyzed using the ImageJ software.

### Quantitative polymerase chain reaction (qPCR) for mRNA and miRNA detection

The peri-infarct tissue samples were collected 3–6 h after reperfusion for detecting the primary *miR-183* cluster (*pri-miR-183/96/182*), or 12–24 h after reperfusion for analysis of mature *miR-183* members and glucose-metabolizing-related proteins, and then quickly frozen in liquid nitrogen. Total RNA was extracted using TRIzol reagent (Vazyme, R401) [12]. The concentration and integrity of the RNA were assessed using a NanoDrop 2000 (Thermo Fisher Scientific), followed by reverse transcription using a HiScript III RT SuperMix for qPCR (+gDNA wiper) kit (Vazyme, R323) according to the manufacturer's instructions. We

performed qPCR on a QuantStudio 3 real-time PCR system (Applied Biosystems, PA, USA) using SYBR qPCR Master Mix (Vazyme, Q711). The primers used are listed in Supplementary Table S2. *Beta-Actin* was used as an internal reference for detection of mRNA, whereas *U6* served as an internal control for the detection of miRNA expression. The  $2^{-\Delta\Delta CT}$  method was used to calculate the fold change.

### Dual-luciferase reporter (DLR) assay of miRNA targets

The 3' untranslated region (UTR) of either WT *Vdac1/2/3* or their MUT forms (Sangon Biotech, Shanghai, China), including the 45-nucleotide sequences with *miR-183* binding sites or the full-length sequences, were inserted into the pmirGLO Dual-Luciferase miRNA Target Expression Vector (Promega, Wisconsin, USA) [12]. HEK293 or HT22 cells were cultured in 24-well plates and transfected with either 50 nM mimics of *miR-183*, *miR-96*, *miR-182*, or *miR-NC* (GenePharma) along with 125 ng of luciferase reporter construct using PEI (Sigma-Aldrich, 40872-7, Darmstadt, Germany). After transfection for 24 h, the cells were collected to measure luciferase activity using a DLR Assay kit (Promega, E1960). The specific sequences of all mimics are listed in Supplementary Table S3.

### 2, 3, 5-triphenyltetrazolium chloride (TTC) staining

Forty-eight and 72 h after reperfusion, mice brains were harvested and frozen at  $-20^{\circ}\text{C}$  for 20 min. The brains were then cut into 1-mm coronal sections, which were subsequently incubated in 2% TTC solution (Solarbio, T8170, Beijing, China) for 10 min at  $37^{\circ}\text{C}$ . After fixation with 4% paraformaldehyde, the size of normal tissues (red) was measured through digital planimetry of the slices by an observer blinded to the experimental conditions utilizing the ImageJ software. To account for the influence of edema in infarct tissues (white), the infarct volume for each brain was calculated using the formula  $I\% = (\text{volume of normal tissues in control hemisphere} - \text{volume of normal tissues in tMCAO hemisphere}) / (2 \times \text{volume of normal tissues in control hemisphere})$ .

### ATP measurement

For in-vivo ATP detection within neuronal cells, an AAV recombinant with synapsin 1 promotor sequence rAAV-hSyn-cyto-iATPSnFR1.0 ( $1 \times 10^9$  viral; Brain Case, Shenzhen, China) that selectively expresses a fluorescent ATP sensor in neurons was injected into the cerebral cortex three weeks before ischemia. Twenty-four hours after reperfusion, iATPSnFR fluorescence responding to ATP binding was

detected under a Zeiss LSM-700 microscope (Oberkochen, Germany).

The ATP content in peri-infarct tissue samples 24 h after reperfusion was measured using an Enhanced ATP Assay Kit (Beyotime, S0027) according to the manufacturer's instructions. Briefly, tissue samples were homogenized with lysis buffer and then centrifuged at  $12,000 \times g$  for 5 min at  $4^{\circ}\text{C}$ . The resulting supernatant was added 5 min after 100  $\mu\text{L}$  of ATP assay working solution had been added to a 96-well opaque plate. Luminescence was measured using a microplate reader (Thermo Fisher Scientific).

### Immunofluorescence (IF) staining

Six and 24 h after reperfusion, whole mice brains for IF staining were fixed with 4% paraformaldehyde, dehydrated with gradient sucrose, embedded in optimal cutting temperature compound, and sectioned at 30  $\mu\text{m}$  using a Leica cryostat. Sections were permeabilized with a solution containing 0.25% Triton X-100 and 1% BSA, and blocked with 10% goat serum albumin for 1 h at room temperature. Primary antibodies were added to the specimens overnight at  $4^{\circ}\text{C}$ , followed by washing thrice with PBS and incubation with secondary antibody for 1 h at room temperature (listed in Supplementary Table S1). The brain slices were observed under a Zeiss LSM-700 microscope.

### Neurological scoring

The modified neurological severity score (mNSS) was used to evaluate a combination of motor, sensory, and balance functions 3, 7, 10, 14, and 21 days after tMCAO, graded on a scale of 0 to 18. Mild, moderate, and severe impairment are indicated by scores between 1 and 6, 7 and 12, and 13 and 18, respectively.

### Behavioral tests

#### Rotarod test

The rotarod test was performed to evaluate motor coordination and muscle endurance. The mice were placed on a rotating rod, which was accelerated from 0 to 40 rpm within 5 min. The time spent on the rod until the mouse fell off was recorded and repeated thrice with at least a 5-min interval between each measurement to calculate the average value. Pre-training for the rotarod, foot-fault, cylinder, and corner tests lasted for 3 days before tMCAO, and data from the third day served as the preoperative baseline.

### Foot-fault test

The foot-fault test was performed to assess forelimb functional coordination. Mice were placed on a 35×35-cm square wire grid with 2.25-cm<sup>2</sup> openings for free movement. The number of missed steps and total steps of the forelimbs on the grid within 2 min were recorded thrice to obtain an average value.

### Cylinder test

The mice were placed in a transparent glass cylinder with a diameter of 9 cm and a height of 12 cm. Data on three scenarios that included climbing the wall of the cylinder in an upright position using the left forelimb (L) only, the right forelimb (R) only, or both forelimbs simultaneously (B) were recorded 20 times, consecutively, to calculate the postoperative preference for using either forelimb. The calculation was performed as follows:  $(R - L) / (L + R + B)$ .

### Corner test

The corner test was used to assess sensorimotor asymmetry in mice after MCAO. Two pieces of cardboard, each measuring 30, 20, and 1 cm in length, height, and thickness, respectively, were set at a 30° angle with a small opening at the joint. The experimental mice were placed between the cardboard pieces and allowed to enter the corner spontaneously. When the vibrissae touched the cardboard and were stimulated, the mouse turned right or left and faced the opening, and the percentage of right turns was calculated.

### Morris water maze

The Morris water maze was used to evaluate hippocampus-dependent spatial navigation learning and memory. The water maze consisted of a circular pool (90 cm diameter) which was divided into four quadrants, filled with water at  $22 \pm 1$  °C until the circular platform (12 cm diameter, 40 cm high) was submerged 1 cm below the surface. Four different clues were set on the pool wall above the water surface to aid spatial navigation. During the learning phase, each mouse was placed in one quadrant randomly to explore for five consecutive days, and the latency to find the hidden platform was recorded, while on the sixth day (memory phase), the platform was moved away and the time spent in the target quadrant and the times crossing the target quadrant within 60 s were recorded. Data were measured and recorded using the ANY-maze software (Stoelting, IL, USA).

### Open-field test

Open-field tests combined with tail suspension and forced swim tests were performed to assess behavioral depression in mice. Mice were placed in a 40×40×40-cm open-field apparatus and allowed to explore freely for 5 min while their exploratory behavioral data, including total and central distance and duration in the center (20×20 cm), were recorded using a video camera with an automated tracking system positioned directly above the field. To maintain cleanliness and consistency between the tests, the field apparatus was cleaned with 75% ethanol at the beginning of each test.

### Tail suspension test

Each mouse was hung at the same height above the floor with an adhesive tape for 6 min. The total time of immobility within the last 4 min was recorded with a fixed camera.

### Forced swim test

Each mouse was allowed to swim randomly for 6 min in a transparent cylinder (17 cm diameter, 27 cm high) filled with water at a height of 12 cm at 23–25 °C. The total immobility duration of each mouse within the last 4 min was recorded, which was defined as floating with hind legs motionless.

### Statistical analysis

The results are presented as the mean  $\pm$  SD unless otherwise specified. Data were from at least three independent experiments or cultures. Statistical analyses were performed using GraphPad Prism 10.0. Comparisons between the two groups were performed using an unpaired *t*-test, with Welch's correction as appropriate. Comparisons among three or more groups were performed using one-way ANOVA followed by Tukey's multiple comparisons or Dunnett's T3 post-hoc tests or two-way ANOVA. Neurobehavioral tests including repeated measures were evaluated using repeated-measures ANOVA, and the results are shown as mean  $\pm$  SEM. Statistical significance was set at  $P < 0.05$  after confirming normality and homogeneity of variance in the data.

## Results

### The transcriptional activity of p53 induces neuronal metabolic dysfunction by downregulating outer mitochondrial membrane protein VDACs after AIS

First, we detected cytosolic ATP levels within neurons 24 h after reperfusion in mice with a fluorescent sensor

rAAV-hSyn-cyto-iATPSnFR1.0 bilaterally transfected in the cerebral cortex. As shown in Fig. 1a and Supplementary Fig. S1a, iATPSnFR in the contralateral (control) cortical neurons showed enhanced fluorescence with physiological ATP levels, whereas cytosolic ATP levels in neurons, specifically in neuronal soma, significantly decreased in the tMCAO cortex 24 h after reperfusion. Neuronal activity (p-CREB) in the tMCAO cortex showed no alteration compared with the control cortex (Fig. 1a). Therefore, a sustained metabolic stress occurs within neuronal cells even with reperfusion following AIS. To investigate the pathological significance of p53-related signaling pathways in neuronal metabolic stress following AIS, we examined the cellular distribution of overexpressed p53 in the mouse brain 6 h after reperfusion. The p53 staining exhibited a small puncta-like distribution in the control cortex, whereas it showed enhanced expression levels and diffused distribution mainly in neuronal cells of the peri-infarct region of the tMCAO cortex (Supplementary Fig. S1b). Then, p53 inhibitors pifithrin- $\alpha$  (PFT- $\alpha$ , 1 mg/kg) and PFT- $\mu$  (8 mg/kg) were used to assess the impacts of p53 transcription-dependent or -independent pathways on ATP levels and neurological damage, respectively (Fig. 1b, Supplementary Fig. S1c, d). The ATP content in the tMCAO tissue was significantly downregulated compared with that in the control cortex 24 h after reperfusion, and such changes were prevented by PFT- $\alpha$  but not PFT- $\mu$  (Fig. 1b). Interestingly, TTC staining showed that PFT- $\alpha$  led to marked reductions in infarct volume after 48 h after reperfusion (Supplementary Fig. S1c). The mNSS analysis showed that neurological functions were impaired after tMCAO but attenuated by PFT- $\alpha$  administration (Supplementary Fig. S1d). PFT- $\mu$  displayed a much lower degree of cerebroprotection compared with PFT- $\alpha$  (Supplementary Fig. S1c, d). These data suggest that excessive p53 triggers a transcriptional program rather than a non-transcriptional response to impair neuronal energy metabolism and neural function after stroke.

Glucose metabolism provides the primary energy source for neurological functions [28, 29]. To investigate the downstream molecular events through which p53 disrupts energy homeostasis, we examined the expression of key glucose-metabolizing enzymes in glycolysis and the pentose phosphate pathway, including hexokinase 1 (HK1), phosphofructokinase 1 (PFK1), lactate dehydrogenase A (LDHA), and glucose-6-phosphate dehydrogenase (G6PD), as well as the mitochondrial functional protein VDAC1/2/3 (Fig. 1c). *Hk1* and *Pfk1* mRNA levels decreased markedly in the tMCAO tissue compared to the control 24 h after reperfusion, whereas *Ldha* and *G6pd* mRNA levels remained stable during 12 and 24 h after reperfusion (Fig. 1d). Unexpectedly, PFT- $\alpha$  administration did not affect the expression of the above genes (Fig. 1e), suggesting that

p53 transcriptional activity may not interrupt glycolytic and pentose phosphate pathways to impair glucose metabolism.

Outer mitochondrial membrane VDACs and inner mitochondrial membrane transporters and translocators function as efficient channels for ATP/ADP and small metabolites, including pyruvate, succinate, and citrate, across mitochondria. Previously, we determined that decreased VDAC1 and VDAC3 levels contribute to ATP decline during the early stages of reperfusion after ischemia [12]. Consistently, the transcripts of the three *Vdac* isoforms were downregulated in the tMCAO cortex during 12 and 24 h after reperfusion (Fig. 1d). Notably, PFT- $\alpha$  reinstated the *Vdac1*, *Vdac2*, and *Vdac3* mRNA levels (Fig. 1f). Immunoblot analysis confirmed that VDAC1 and VDAC3 levels reduced 24 h after reperfusion, whereas this change was prevented by PFT- $\alpha$  but not PFT- $\mu$  (Fig. 1g). Stable cytochrome c oxidase subunit 4 (COX4) levels suggest no reduction in mitochondrial number during the early stages of I/R (Fig. 1g). These results indicate that I/R induces a p53 transcriptional response to inhibit neuronal energy metabolic processes by downregulating the mitochondrial functional protein VDACs after AIS.

### Neuronal p53 is responsible for post-stroke neurocognitive impairments and depression-like behaviors in mice

Next, we investigated the pathological significance of neuronal p53 signaling in neuropsychiatric disturbances following AIS. To avoid neurodevelopmental abnormality, the adult *Trp53<sup>fllox/fllox</sup>* mice were injected with AAV-CaMKII $\alpha$ -Cre recombinants to specifically knockout the *Trp53* gene in mouse cortical neurons (Fig. 2a). IF staining revealed a specific ablation of neuronal p53 in the CaMKII $\alpha$ -Cre groups but not its negative control (CaMKII $\alpha$ -NC) groups 24 h after reperfusion (Fig. 2b). Compared to the CaMKII $\alpha$ -NC groups, long-term neurofunctional deficits were mitigated in the CaMKII $\alpha$ -Cre groups (Fig. 2c). Sensorimotor behavioral tests, including the rotarod, foot-fault, and cylinder tests, showed that the CaMKII $\alpha$ -Cre groups exhibited sustained improvements in sensorimotor function recovery (Fig. 2d-f). In the Morris water maze test, the mice with neuronal p53 ablation showed improved spatial memory after I/R (Fig. 2g), but no alteration in spatial learning ability and swimming speed (Supplementary Fig. S2a-c). Interestingly, neuronal p53 ablation alleviated depression-like behaviors in mice during the open-field (Fig. 2h), tail suspension (Fig. 2i), and forced swim tests (Fig. 2j). These findings suggest that targeting neuronal p53 signaling supports neurocognitive function recovery and emotional regulation after AIS.



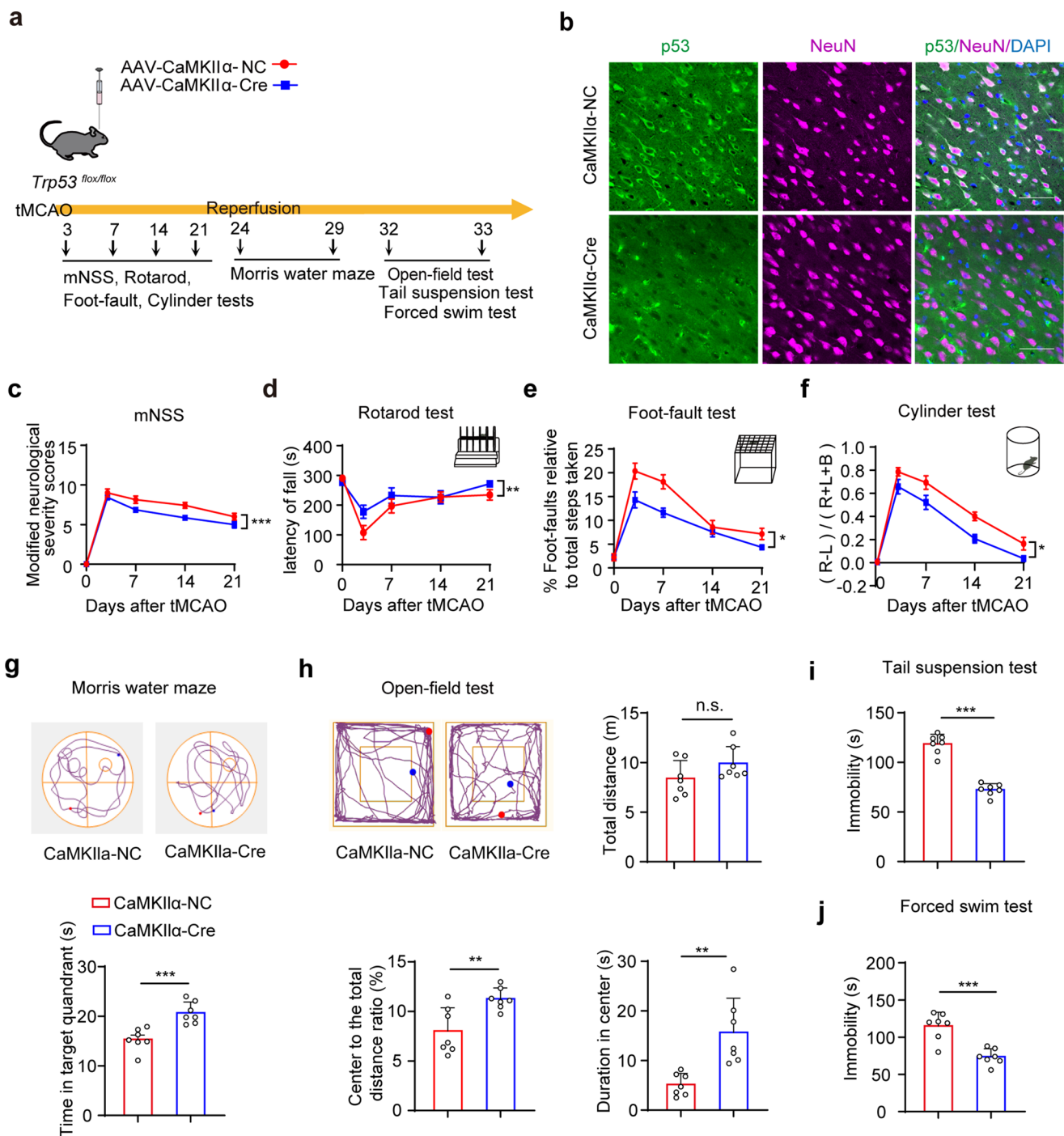


**Fig. 2** Neuronal p53 ablation ameliorates sensorimotor, spatial memory, and depressive behaviors in mice after tMCAO. **(a)** Schematic experimental timeline of neurological and behavioral tests in *Trp53<sup>fllox/fllox</sup>* mice with conditional knockout of p53 in neurons through injection of AAV-CaMKII $\alpha$ -Cre or its negative control (AAV-CaMKII $\alpha$ -NC). **(b)** IF staining for p53 expression in the peri-infarct region of the tMCAO cortex 24 h after reperfusion in mice injected with AAV-CaMKII $\alpha$ -Cre or its negative control. Co-staining with NeuN marks neurons (including 12 slices from four mice). Scale bar = 50  $\mu$ m. **(c–f)** Assessment of mNSS for long-term neurological deficits **(c)** and sensorimotor behavioral tests, including rotarod **(d)**, foot-fault **(e)**, and cylinder **(f)** tests, 3, 7, 14, and 21 days after reperfu-

sion after tMCAO. Data are shown as the mean  $\pm$  SEM ( $n=7$  mice) and were analyzed using two-way ANOVA with repeated measures. \* $P<0.05$ ; \*\* $P<0.01$ ; \*\*\* $P<0.001$ . **(g)** Analysis of the time in the target quadrant during the memory phase approximately 24 to 29 days after tMCAO in the Morris water maze. **(h)** Analysis of the open-field test approximately 32 days after reperfusion after tMCAO, including representative tracks, total distance, central distance, and time in the center. **(i and j)** Quantitation of immobility time in the tail suspension test **(i)** and forced swim test **(j)** approximately 32 to 33 days after reperfusion. Data are shown as the mean  $\pm$  SEM ( $n=7$  mice) and were analyzed using unpaired *t*-tests **(g–j)**. \*\* $P<0.01$ ; \*\*\* $P<0.001$ ; n.s., not significant



## Neuronal p53 transactivates and boosts miR-183 cluster after AIS

How does neuronal p53 transcriptional activity induce post-stroke metabolic stress and neuropsychiatric symptoms? As no *cis*-regulatory elements required for p53-directed regulation are found in the upstream promoter region (UPR) of *VDACs*, we hypothesized that p53 transcripts are *miRNAs* that post-transcriptionally interfere with the expression of downstream *VDACs*. Bioinformatics analysis predicted *miR-183* as a candidate mediator. The *miR-183-5p* (*miR-183*) together with *miR-96-5p* (*miR-96*) and *miR-182-5p* (*miR-182*) comprises a polycistronic paralogous cluster that is generated from a single primary *miRNA* (*pri-miR-183/96/182*). Putative response elements (PREs) for p53 in the UPR of the *miR-183* cluster are highly conserved among humans, rats, and mice (Supplementary Fig. S3a). To identify whether p53 enhances the promoter activity of the *miR-183* cluster, we constructed two luciferase reporter recombinant containing the mouse *miR-183* cluster UPR1 (-3000 to -1600) or UPR2 (-1600 to -1). A recombinant containing the p53-responded UPR of mouse *Cdkn1a/p21* was the positive control. The DLR assay in HT22 neuronal cells showed that the *miR-183* UPR1 recombinant yielded the same robust transcriptional activity as the *Cdkn1a* UPR, and this activity was almost completely abolished by PFT- $\alpha$  (Supplementary Fig. S3b). Additionally, the p53-responded PRE(WT) in the *miR-183* cluster and its MUT were cloned into luciferase reporter vectors (Fig. 3a). The luciferase activity of the PRE(MUT) was much lower than that of PRE(WT) (Fig. 3b), confirming that p53 transactivates the promoter of the *miR-183* cluster. Furthermore, OGD/R in HT22 neuronal cells augmented luciferase activity of PRE(WT) (Fig. 3c), suggesting that OGD/R-induced neuronal p53 transcriptionally regulates the *miR-183* cluster. Next, we examined the *in-vivo pri-miR-183/96/182* levels 3 and 6 h after reperfusion (Fig. 3d) and three mature members (*miR-183*, *miR-96*, and *miR-182*) at 12 and 24 h after reperfusion (Fig. 3e) and found that they were much greater and sustained in the mouse tMCAO cortex than in the control tissue. PFT- $\alpha$  (1 and 2 mg/kg) markedly reduced the *pri-miR-183/96/182* levels 3 h after reperfusion, whereas PFT- $\mu$  and the vehicle showed no effect (Fig. 3f). Consistently, PFT- $\alpha$  (1 mg/kg) abolished postischemic upregulation of mature *miR-183* members 24 h after reperfusion (Fig. 3g).

We subsequently determined the *in-vivo* regulation of the *miR-183* cluster by AIS-induced neuronal p53, and the results showed that *pri-miR-183/96/182* levels and three mature members (*miR-183*, *miR-96*, and *miR-182*) increased after tMCAO in control (CaMKII $\alpha$ -NC) mice but showed no alteration in neuronal p53 ablation (CaMKII $\alpha$ -Cre) mice (Fig. 3h, i). In addition, we observed a consistent decrease

in *pri-miR-183/96/182* levels in *Trp53* null mice (Supplementary Fig. S4a, b). In contrast, p53 conditional knockout in mouse astroglia by infusion with AAV-GFAP-Cre did not notably eliminate elevated *pri-miR-183/96/182* after tMCAO, and only a slight decline was observed (Supplementary Fig. S4c, d). These findings indicate that neuronal p53 boosts the transcription and biogenesis of the *miR-183* members after I/R.

## Vdac transcripts are directly decreased by miR-183 and miR-96

The *miR-183* family members are highly conserved across mammalian species (Fig. 4a). The *miR-183* and *miR-96* were predicted to bind with the *Vdac1/2/3* mRNA 3' UTR and *Vdac3* mRNA 3' UTR, respectively (Fig. 4b). The DLR assay showed that *miR-183* mimics suppressed the luciferase activity of 3' UTR constructs of *Vdac1/2/3* in HEK293 cells, and did not affect the luciferase activity of their mutants (Fig. 4c, d). To further investigate the difference in targeted action of various *miR-183* family members, we transfected HT22 neuronal cells with the full-length 3' UTR constructs of *Vdac1/2/3* (Fig. 4e). The *miR-183* mimics had similar inhibitory effects on the relative luciferase activities of *Vdac1*, *Vdac2*, and *Vdac3* (Fig. 4f). In addition to the similar predicted target regulation of *Vdac3*, *miR-96* mimics also reduced the relative luciferase activity of *Vdac1* (Fig. 4g). As expected, *miR-182* mimics did not significantly change the luciferase activity of *Vdacs* (Fig. 4h). Thus, *miR-183* family members, except *miR-182*, directly target and downregulate *VDAC* expression.

## Neuronal p53 induces mitochondrial and neurological deficits through the miR-183 cluster pathway

Furthermore, we investigated the involvement of p53-elicited *miR-183* family transcripts in post-stroke *VDAC* decline and its pathophysiological processes. The *miR-183* mimics or *miR-NC* were infused into the lateral ventricles of neuronal p53 conditional knockout mice (CaMKII $\alpha$ -Cre groups) after tMCAO (Fig. 5a). The *VDAC1* and *VDAC3* levels significantly decreased in the CaMKII $\alpha$ -NC groups 24 h after reperfusion. Notably, neuronal p53 ablation restored *VDAC1* and *VDAC3* levels in the *miR-NC* groups, which was reversed in the *miR-183* mimic groups (Fig. 5b). Correspondingly, neuronal p53 loss restored ATP levels in the tMCAO cortex, whereas the rescue of *miR-183* expression terminated such benefits (Fig. 5c). Conditional knockout of neuronal p53 dramatically diminished the infarct size and mNSS scores 48 h after reperfusion; however, both effects were diminished by *miR-183* mimics (Fig. 5d, e). These data

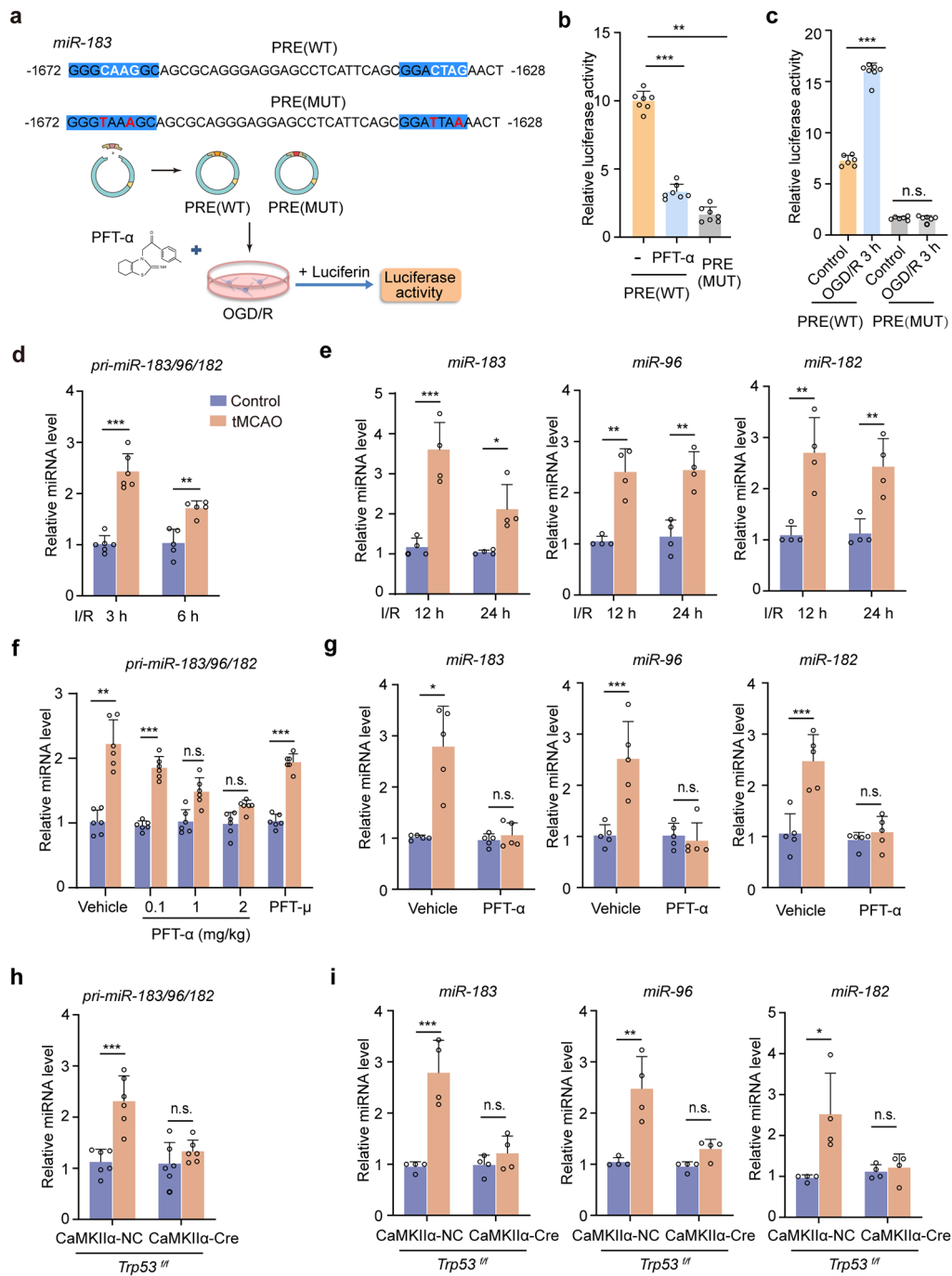


**Fig. 3** Neuronal p53 ablation decreases the transcripts of the *miR-183* cluster after tMCAO. **(a)** Sequence showing the location of PRE for p53 in the WT *miR-183* cluster. MUT introduced into the promoter reporter construct are shown in red. **(b)** Dual-luciferase reporter assay of the promoter activity of WT and MUT PRE for p53 in the *miR-183* cluster in HT22 neuronal cells treated with or without PFT- $\alpha$  (5  $\mu$ M;  $n=7$ , from at least three independent cultures). **(c)** Dual-luciferase reporter assay of the promoter activity of WT and MUT PRE for p53 in the *miR-183* cluster in HT22 neuronal cells after OGD/R ( $n=6$  or 7, from at least three independent cultures). Relative luciferase activity was normalized to that of the pGL3-basic groups **(b and c)**. **(d and e)** Relative *pri-miR-183/96/182* **(d)** and *miR-183* family member (*miR-*

*183*, *miR-96*, and *miR-182*) **(e)** levels in the mouse peri-infarct region of the tMCAO cortex and contralateral control cortex (qPCR;  $n=4-6$ ). **(f and g)** Relative *pri-miR-183/96/182* levels 3 h after reperfusion **(f)** and *miR-183* family member levels 24 h after reperfusion **(g)** in mice administrated the vehicle, PFT- $\alpha$  (0.1, 1, and 2 mg/kg), or PFT- $\mu$  (8 mg/kg) (qPCR;  $n=5$  or 6). **(h and i)** Relative *pri-miR-183/96/182* levels 3 h after reperfusion **(h)** and *miR-183* family member levels 24 h after reperfusion **(i)** in neuronal p53 ablation mice (qPCR;  $n=4$  or 6). Data are shown as the mean  $\pm$  SD and were analyzed using two-way ANOVA **(b-c and h-i)** or one-way ANOVA **(d-g)**. \* $P<0.05$ ; \*\* $P<0.01$ ; \*\*\* $P<0.001$ ; n.s., not significant

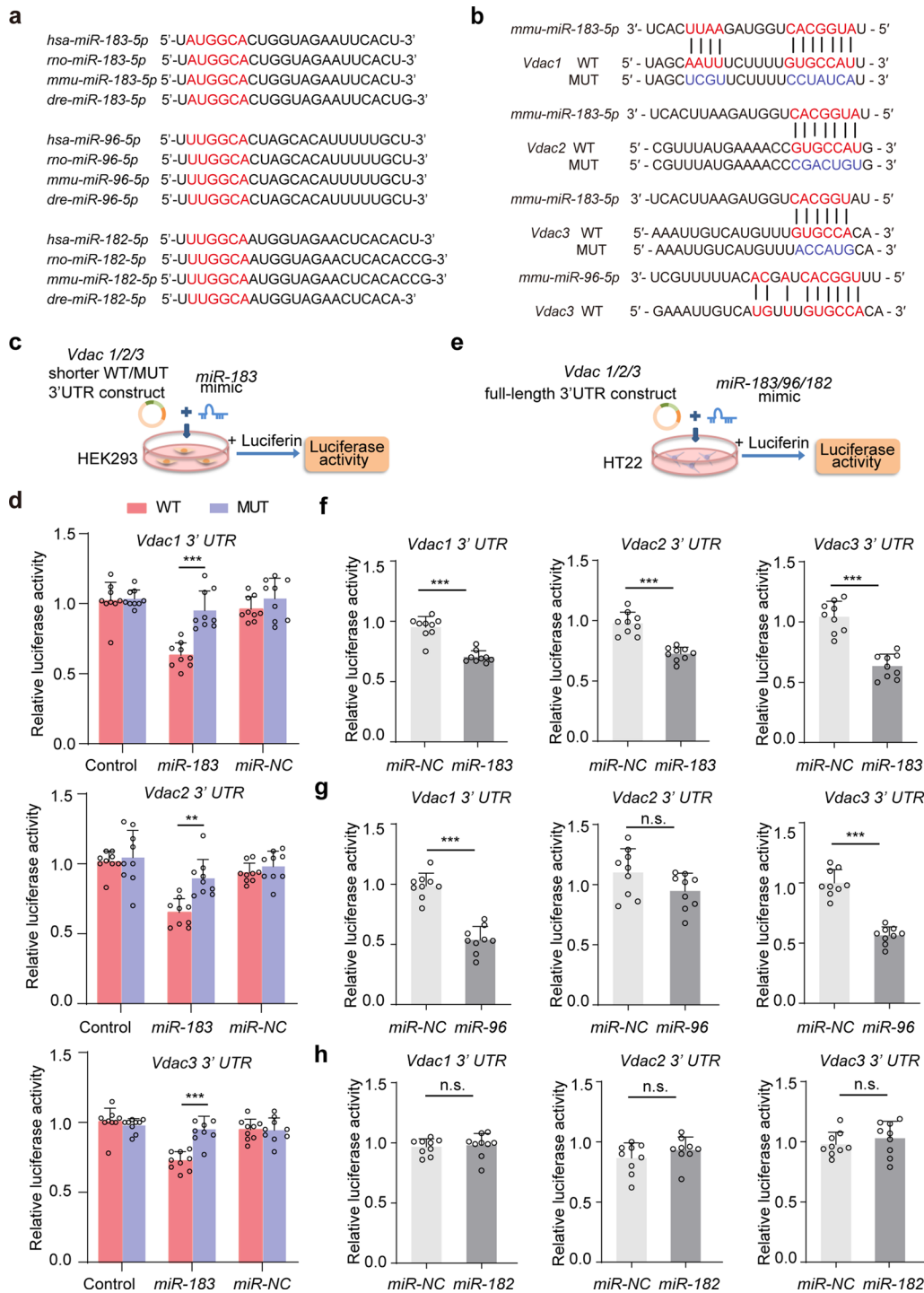


**Fig. 4** *miR-183* and *miR-96* directly target the 3' UTR region of *Vdacs*. (a) Highly conserved *miR-183* family members (*miR-183-5p*, *miR-96-5p*, and *miR-182-5p*) among *Homo sapiens* (*hsa*), *Rattus norvegicus* (*rno*), *Mus musculus* (*mmu*), and *Danio rerio* (*dre*). Seed sequences are shown in red. (b) Potential binding sites of *mmu-miR-183-5p* are shown targeting the WT (red) or MUT (blue) 3' UTR region of *Vdac1/2/3*, whereas those of *mmu-miR-96-5p* are shown targeting the 3' UTR region of *Vdac3* mRNA. (c and d) Dual-luciferase reporter assays in HEK293 cells were performed by transfecting blank control, *miR-183* mimics (*miR-183*), or its negative control (*miR-NC*) together with the luciferase reporter constructs carrying 3' UTR (WT

or MUT) of *Vdac1/2/3*, respectively (c). Relative luciferase activity was inhibited by *miR-183* mimics in the *Vdac1/2/3* WT groups but not their MUT groups, respectively (d). (e–h) Schematic protocol of dual-luciferase reporter assays in HT22 neuronal cells (e). HT22 cells were co-transfected with *miR-NC* or mimics of *miR-183* (f), *miR-96* (g), or *miR-182* (h) with the luciferase reporter constructs carrying the full-length 3' UTR region of *Vdac1/2/3*, respectively. Relative luciferase activity was normalized to that of the control groups. Data are shown as the mean ± SD (*n* = 9) and were analyzed using one-way ANOVA (d) or unpaired *t*-tests (f–h). \*\**P* < 0.01; \*\*\**P* < 0.001; n.s., not significant

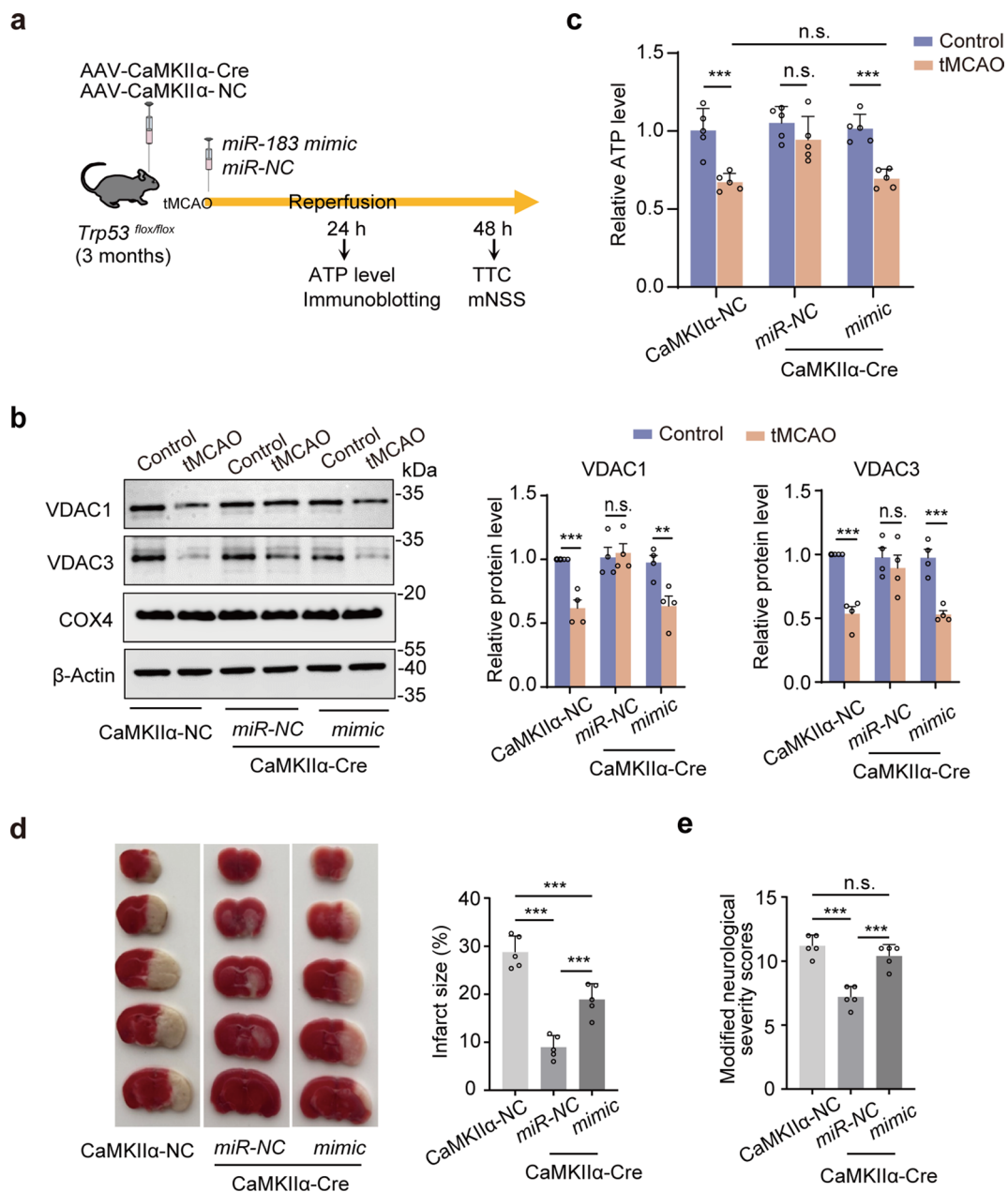


**Fig. 5** Rescue of *miR-183* reverses p53 ablation-induced recovery from VDACs/ATP decline and cerebral infarction. **(a)** Schematic diagram of the experimental flow. Neuronal p53 was selectively ablated by infusion with AAV-CaMKII $\alpha$ -Cre in adult *Trp53*<sup>flax/flax</sup> mice; AAV-CaMKII $\alpha$ -NC infusion served as a negative control. The *miR-183* mimics (300 pmol) were treated 50 min after tMCAO. **(b)** Immunoblotting assessment of VDAC1, VDAC3, and COX4 levels in the peri-infarct cortex of tMCAO and contralateral control tissues 24 h after reperfu-

sion. Beta-Actin was used as a loading control ( $n=4$ ). **(c)** Relative ATP levels in the peri-infarct cortex of tMCAO and contralateral control tissues 24 h after reperfusion ( $n=5$ ). **(d)** TTC analysis and quantification of cerebral infarct size 48 h after reperfusion ( $n=5$ ). **(e)** mNSS assessment for neurological deficits 48 h after reperfusion ( $n=5$ ). Data are shown as the mean  $\pm$  SD and were analyzed using two-way ANOVA. \* $P < 0.05$ ; \*\* $P < 0.01$ ; \*\*\* $P < 0.001$ ; n.s., not significant

suggest that neuronal p53 impairs energy metabolism and that neurological deficits occur in mice through transcriptional regulation of the *miR-183* family/VDAC axis after I/R.

### Neuronal CDK9 is activated and induces ATP decline via the p53/VDAC pathway

To identify a druggable target for AIS treatment, we sought to investigate an upstream regulator of the p53 transcriptional program in neuronal cells following I/R. The DLR

assay showed that OGD/R boosted the p53-binding promoter activity of the *miR-183* cluster in HT22 neuronal cells; this activity was blocked by post-treatment with the small-molecule CDK9 inhibitor oroxylin A, suggesting that neuronal CDK9 activation enhances p53 transcriptional response (Fig. 6a, b). Although CDK9 downregulates p53 levels through MDM2/sirtuin 1 signaling in cancer cells [30, 31], the distribution and pathophysiological roles of CDK9 in the mammalian brain remain poorly understood. In this study, IF staining showed that CDK9 was particularly enriched in cortical neurons (Fig. 6c). As expected, oroxylin A (10 mg/kg) treatment 30 min after tMCAO reversed ATP decline within neurons and facilitated ATP production 24 h after reperfusion (Fig. 6d, e), and markedly attenuated cerebral infarction compared with the vehicle groups 72 h after reperfusion (Fig. 6f).

Oroxylin A posttreatment not only inhibited CDK9 activity but also partially reversed the overexpression of p53 24 h after reperfusion (Fig. 7a, b). In addition, oroxylin A reduced the upregulated levels of *miR-183*, *miR-96*, and *miR-182* 24 h after reperfusion (Fig. 7c), and blocked the post-ischemic decline in VDAC1, VDAC2, and VDAC3 (Fig. 7d, e). Similar effects of oroxylin A posttreatment on the expression of CDK9, p53, VDAC1, and VDAC3 were observed in female mice (Supplementary Fig. S5a, b). Therefore, unlike its roles in cancer cells, neuron-enriched CDK9 augments the intrinsic p53 transcriptional response, which is responsible for ATP decline after stroke.

### Oroxylin A therapy ameliorates long-term outcomes after AIS

Finally, we investigated the therapeutic significance of oroxylin A in neuropsychiatric abnormalities following AIS (Fig. 8a). The mNSS and sensorimotor behavioral tests, including the rotarod, foot-fault, cylinder, and corner tests, showed that oroxylin A (10 mg/kg) posttreatment for three times provided long-term benefits for neurological function recovery (Fig. 8b-f). In addition, oroxylin A posttreatment reversed spatial memory deficits in the water maze test (Supplementary Fig. S6a-e); no obvious difference in spatial learning and swimming speed between the oroxylin A- and vehicle-treated groups were observed (Supplementary Fig. S6a-c). Moreover, oroxylin A reduced brain atrophy 33 days after reperfusion compared to the vehicle group (Supplementary Fig. S6f). Unexpectedly, short-term therapy with oroxylin A did not recover PSD in mice. However, long-term therapy with oroxylin A (5 mg/kg) for 12 days (Fig. 8g) markedly alleviated mouse depression-like behaviors after stroke in the open-field (Fig. 8h), tail suspension (Fig. 8i), and forced swim (Fig. 8j) tests. Thus, oroxylin A is

a potential therapeutic drug for improving long-term post-stroke outcomes.

## Discussion

Understanding the critical molecular regulators underlying aberrant energy metabolism may provide novel drug-gable targets and develop drug interventions for post-stroke neuropsychiatric symptoms. In the present study, we reveal that the p53 transcriptional response, but not its transcription-independent function, drives bioenergy decline within neurons following AIS. Mechanistically, the I/R-induced neuron-intrinsic CDK9/p53/*miR-183* cluster signaling pathway downregulates functional VDACS in the mitochondria, thereby interfering with energy metabolism. This study reveals the therapeutic potential of oroxylin A in providing energy support and ameliorating PSCI and PSD.

Our data showed that the transcriptional program of p53 disrupts neuronal mitochondrial energy metabolism and aggravates progressive cerebral infarction, which is closely linked to long-term disability, neuropsychiatric complications, and even modality in patients with AIS. The stability of the neuronal bioenergy supply is critical for synaptic transmission and plasticity, calcium homeostasis, and neuronal survival [10, 12, 13]. Therefore, the transcriptional suppression of p53 confers robust cerebroprotection against secondary injury and promotes neurological functional recovery by maintaining bioenergy homeostasis. Although cancer cell-intrinsic p53 negatively modulates aerobic glycolysis (the Warburg effect), which fuels tumor growth and progression [32, 33], how excessive p53 reprograms energy metabolism in the mammalian brain remains poorly understood. The present study provides novel evidence that neuronal p53 transcriptionally regulates *miR-183* and *miR-96* biogenesis, which in turn targets the mitochondrial functional protein VDAC, ultimately blocking the tricarboxylic acid cycle and oxidative phosphorylation pathways after AIS. In addition to stroke, upregulation of p53 expression or its transcriptional activity are also involved in the development of neurodegenerative disorders, including Alzheimer's disease and Parkinson's disease [20, 34, 35], providing possibilities for CDK9-targeting interventions in clinical treatment of neurodegenerative diseases.

VDACS in the outer mitochondrial membrane act as primary transporters of ions and metabolites [36, 37]. We elucidated that stabilized VDAC levels improved early mitochondrial energy metabolism after I/R, suggesting that intrinsic VDACS play an indispensable role in neuronal ATP generation. Neurons have a relative lower glycolytic flux in contrast to astrocytes [38], and their axon terminals prefer to mitochondrial oxidative phosphorylation [29]. Therefore,

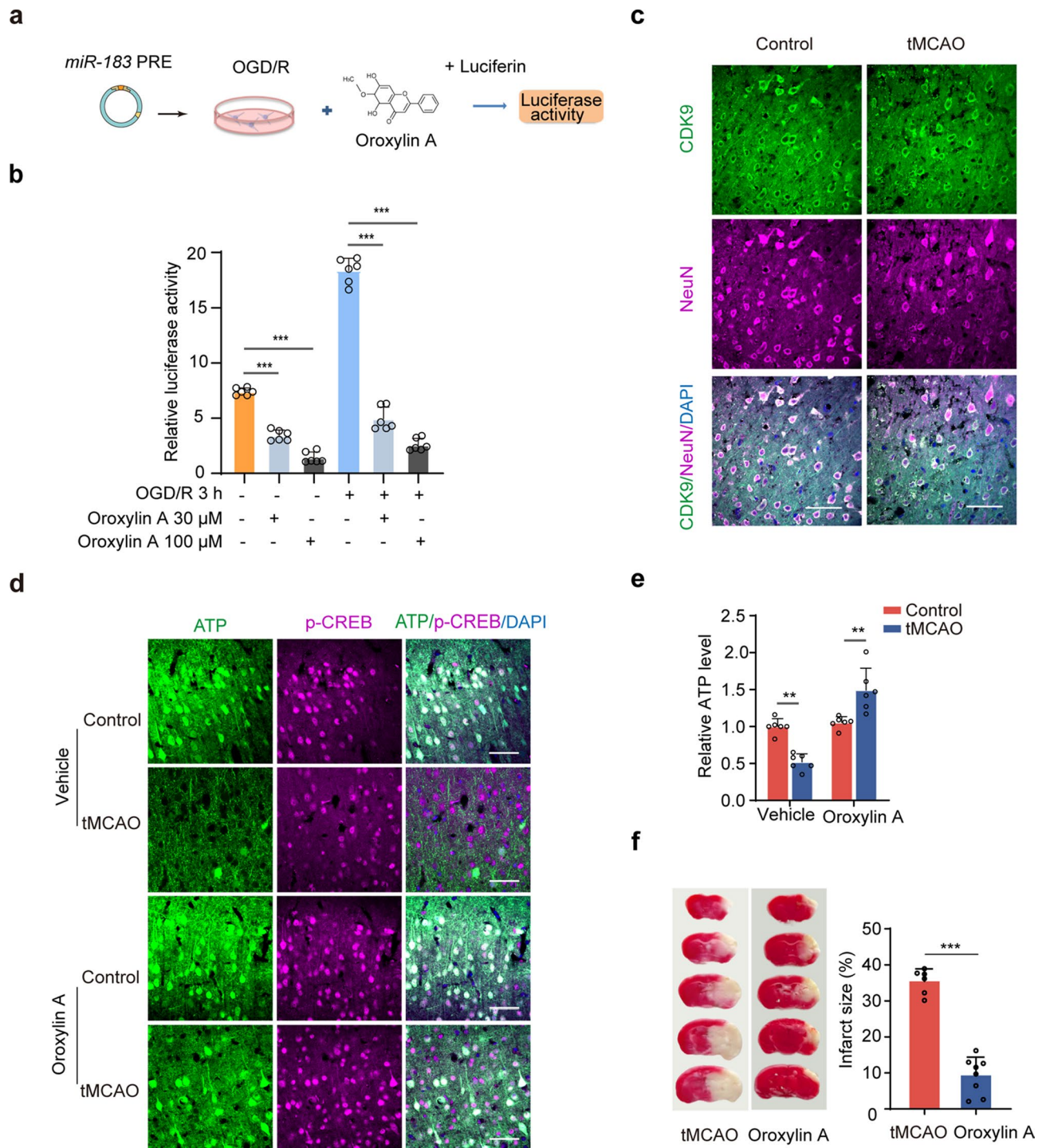


**Fig. 6** CDK9 enhances p53 transcriptional activity in neurons and inhibits ATP production in neurons after tMCAO. (a and b) Dual-luciferase reporter assay of p53-responed promoter activity of the *miR-183* cluster in HT22 neuronal cells after OGD/R. HT22 cells were treated with roxylin A (30 or 100  $\mu$ M) after OGD (a). Relative luciferase activity was normalized to the pGL3-basic groups (b;  $n=6$ , from at least three independent cultures). (c) Immunofluorescence staining of CDK9 distribution in the peri-infarct cortex (tMCAO) and its contralateral region (control) 24 h after reperfusion. Co-staining with NeuN marks neurons (including 15 slices from three mice). Scale bar

= 50  $\mu$ m. (d) Neuronal ATP levels of in tMCAO and control 24 h after reperfusion. Co-staining with p-CREB indicates neuronal activity (including 15 slices from three mice). Scale bar = 50  $\mu$ m. (e) Relative ATP levels were measured in mice post-treated with vehicle or oroxylin A 24 h after reperfusion ( $n=6$ ). (f) TTC analysis and quantification of cerebral infarct size 3 days after tMCAO ( $n=6$  vehicle, and  $n=8$  oroxylin A). Data are shown as the mean  $\pm$  SD and were analyzed using one-way ANOVA (b and e) or unpaired *t*-tests (f). \*\* $P < 0.01$ ; \*\*\* $P < 0.001$

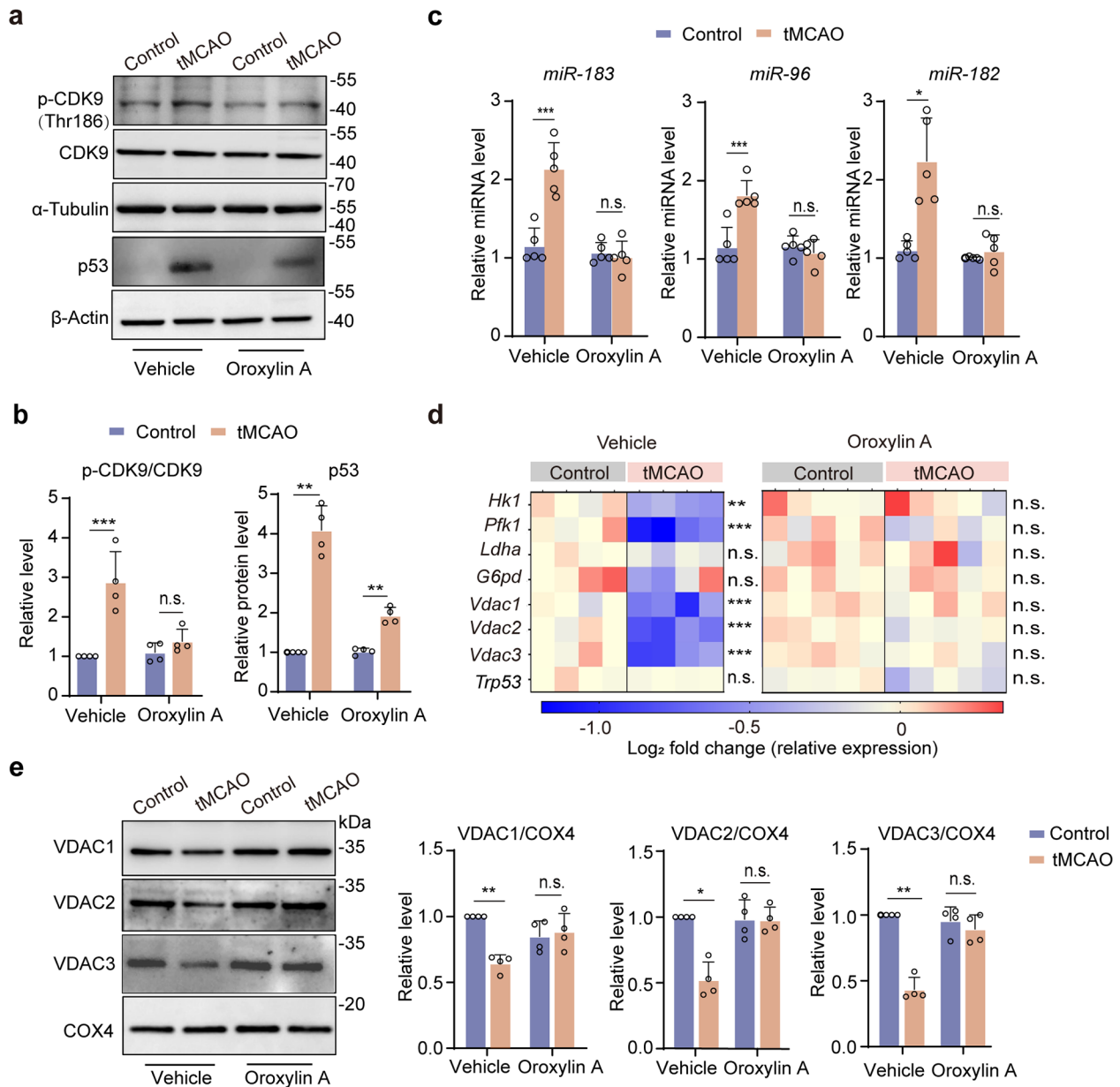


**Fig. 7** CDK9 inhibition by oroxylin A restrains p53/VDAC cascades in mice after tMCAO. (**a** and **b**) Immunoblotting assessment of CDK9 (phosphorylated and total protein) and p53 levels 24 h after reperfusion in mice post-treated with vehicle or oroxylin A (10 mg/kg). Beta-Actin and  $\alpha$ -Tubulin were served as loading controls ( $n=4$ ). (**c**) Relative *miR-183* family member levels (*miR-183*, *miR-96*, and *miR-182*) in the peri-infract tissues of tMCAO and contralateral control cortex 24 h after reperfusion in mice post-treated with vehicle or oroxylin A (qPCR;  $n=5$ ). (**d**) Heatmap showing expression of the key proteins

of the glucose-metabolizing process and *Trp53* at the mRNA levels (qPCR;  $n=4$  vehicle, and  $n=5$  oroxylin A) in the peri-infract region of the tMCAO and contralateral cortexes 24 h after reperfusion. (**e**) VDAC1, VDAC2, and VDAC3 levels (immunoblotting;  $n=4$ ) 24 h after reperfusion in mice after treatment with vehicle or oroxylin A. COX4 served as the loading control. Data are shown as the mean  $\pm$  SD and were analyzed using one-way ANOVA. \* $P < 0.05$ ; \*\* $P < 0.01$ ; \*\*\* $P < 0.001$ ; n.s., not significant

stabilized VDACS in neurons maintain mitochondrial oxidative phosphorylation to support calcium buffering, neurotransmission, and network remodeling following AIS. Interestingly, VDAC1 regulates mitophagy, thereby playing a neuroprotective role in subarachnoid hemorrhage [39–41]. Notably, mitophagy selectively clears damaged

mitochondria, suggesting a therapeutic strategy to alleviate neurological dysfunction by strengthening mitophagy. However, mitophagy is suppressed during early reperfusion following cerebral ischemia [42, 43]. We inferred that a sustained decline in VDAC expression suppressed the clearance of dysfunctional mitochondria through mitophagy.

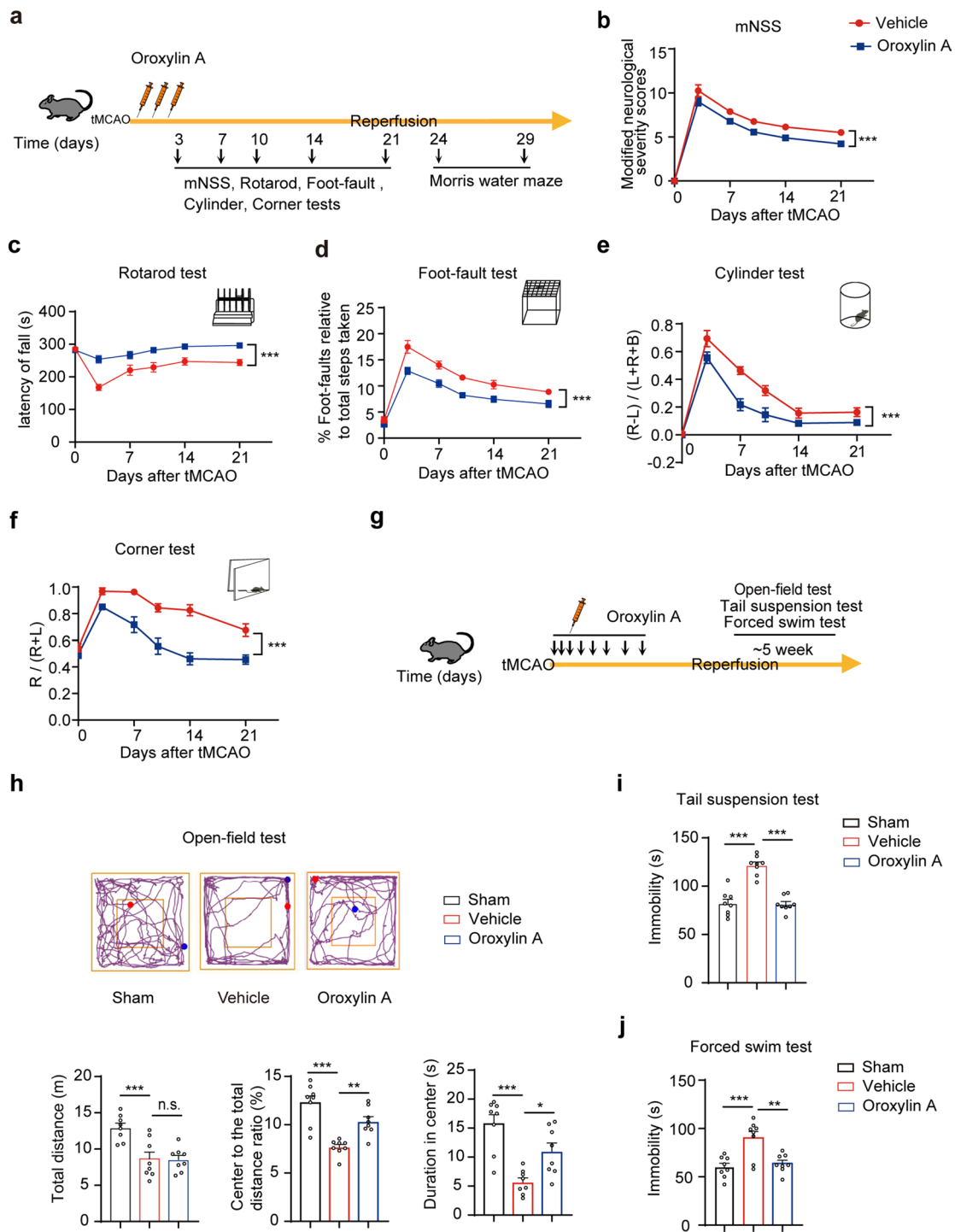


**Fig. 8** Oroxylin A therapy improves long-term sensorimotor, spatial cognitive, and depressive behaviors in mice after tMCAO. **(a)** Schematic experimental timeline of neurological and behavioral tests in mice treated with Oroxylin A (10 mg/kg/d, thrice) or its vehicle 30 min after tMCAO. **(b–f)** Assessment of mNSS for long-term neurological deficits **(b)** and sensorimotor behavioral tests, including rotarod **(c)**, foot-fault **(d)**, cylinder **(e)**, and corner **(f)** tests 3, 7, 10, 14, and 21 days after tMCAO. Data are shown as the mean ± SEM ( $n=8$  vehicle, and  $n=9$  Oroxylin A) and were analyzed using two-way ANOVA with repeated measures. \*\*\* $P<0.001$ . **(g)** Schematic experimental timeline of drug administration and long-term behavioral tests. Mice were

treated with Oroxylin A (5 mg/kg) or its vehicle 30 min after tMCAO for the first administration, then at 1, 2, 4, 6, 8, 10, and 12 days after tMCAO. **(h)** Analysis of open-field test results approximately 5 weeks after tMCAO, including representative tracks, total distance, central distance, and time in the center. **(i and j)** Quantitation of immobility time in the tail suspension test **(i)** and forced swim test **(j)** approximately 5 weeks after tMCAO. Data are shown as the mean ± SEM ( $n=8$  vehicle, and  $n=8$  Oroxylin A) and were analyzed using one-way ANOVA **(h–j)**. \* $P<0.05$ ; \*\* $P<0.01$ ; \*\*\* $P<0.001$ ; n.s., not significant



Our previous findings indicated that I/R induces *miR-7* to downregulate VDACs [12]. However, p53 does not transactivate *pri-miR-7-1* and *pri-miR-7-2* after tMCAO. We determined that upregulation of the *miR-183/96/182* cluster by p53 is detrimental to mitochondrial metabolism and neurological functional recovery after AIS. Three members of the *miR-183* family, which are highly conserved among mammalian species, exhibit similar seed sequences, cluster locations, and expression patterns at different developmental stages [44]. The clustering features may sustain their stability and efficiency and cooperatively induce broad downstream signal events. The *miR-183/96/182* cluster is coordinately involved in neurosensory, cognitive, and circadian regulatory functions [45–48]. However, its neurophysiological and pathological significance and underlying mechanisms are not yet completely understood. The *miR-183* and *miR-96* are responsible for the post-stroke decline of VDACs, whereas *miR-182* might act on other targets in the same context because of minor differences in the seed sequence. A previous study showed that *miR-182* overexpression decreases the synapse-enriched proteins cortactin and Rac1 in the amygdala and impairs long-term fear memory [46]. Furthermore, *miR-182* is negatively correlated with the long-term potentiation-related CREB/BDNF pathway in the hippocampus [49]. Therefore, the I/R-induced overexpression of neuronal *miR-182* may impair synaptic plasticity and cause long-term cognitive deterioration. Additionally, *miR-182* biogenesis increases in the brain after tMCAO and in astrocytes after OGD/R, which may be associated with astrocytic bioenergetic control [50]. PETN has been identified as a target of *miR-183* in Neuro-2 A cells [51], whereas PTEN keeps protein levels stable in the brain during tMCAO/R [52], suggesting that PTEN is not a major endogenous target of *miR-183* after stroke. The multifunctional cytokine oncostatin M provides endogenous protection against ischemic cerebral injury [53]. Evidence indicated that *miR-183* directly targets the neuronal oncostatin M receptor [54]. Post-stroke upregulated *miR-183* levels may resist the neuroprotective effects of oncostatin M. Our study bridges the molecular gaps in p53/*miR-183* family/VDAC signaling following I/R and suggests that the *miR-183/96/182* cluster is a potential molecular target for cerebroprotection.

Interestingly, we determined that overactivated CDK9 acts as an upstream positive regulator of the p53/*miR-183* family/VDAC axis. Excessive CDK9 activity directly promotes OGD/R-induced neuronal p53 transcriptional activity and also facilitates p53 expression in cortical neurons after AIS. In contrast, CDK9 is negatively correlated with p53 levels in human cancer tissues and cells [31, 55]. CDK9 phosphorylates MDM2 and the NAD-dependent deacetylase sirtuin 1, indirectly leading to p53 degradation in

human hepatoma cells [31]. These data suggest that CDK9 regulation of p53 signaling is cellular context-dependent. However, the neurophysiological roles and pathological consequences of CDK9 require further investigation.

Our data revealed that the CDK9/p53 transcriptional signaling cascade represents a potential drug target for AIS treatment. Notably, p53 transcriptional activity inhibitors might pose potential tumorigenicity risks, even though the transcription-independent program of p53 plays a pivotal role in suppressing tumorigenesis [25–27]. Considering that oroxylin A displays anticancer pharmacological activity, we evaluated the therapeutic effects of the small-molecule CDK9 inhibitor oroxylin A on post-stroke acute neurological damage and long-term neuropsychiatric outcomes. Additionally, oroxylin A is able to cross the blood-brain barrier and its safety has been verified [56–58]. To avoid relatively low oral bioavailability due to the significant first-pass metabolism of oroxylin A, we administered this drug to mice through intravenous injection. Oroxylin A has already been shown to attenuate the hypoperfusion-induced cognitive dysfunction in a cerebral small-vessel disease mouse model and ischemic optic neuropathy in rats [59, 60]. Our data provide evidence that oroxylin A therapy not only improves post-stroke sensorimotor abilities but also alleviates PSCI and PSD through providing bioenergetic support.

Although we showed that excessive p53 expression is mainly induced in peri-infarct cortical neurons following ischemic stroke, the roles of the CDK9/p53 axis in glial cells require further investigation. In addition, *Hk1* and *Pfk1* mRNA levels are downregulated in the peri-infarct cortex after tMCAO. HK1 and PFK1 catalyze the first and second key steps of glycolysis, respectively. Further experiments are required to determine whether and how a decline in HK1 and PFK1 levels contributes to ischemic brain disorders. In addition, a limitation of our study is that we used a mouse hippocampal cell line rather than primary neuronal cultures. The lack of studies in females and clinically relevant aged mice is an additional limitation.

In conclusion, our findings reveal the regulatory mechanism responsible for aberrant energy metabolism and its link with post-stroke neurocognitive and emotional disorders. The present study highlights that a novel CDK9/p53/*miR-183* cluster/VDAC signaling cascade underlies progressive neurological impairments and long-term poor outcomes after AIS, and revealed that the CDK9 inhibitor oroxylin A has therapeutic potential against PSCI and PSD.

**Supplementary Information** The online version contains supplementary material available at <https://doi.org/10.1007/s00018-024-05428-4>.

**Acknowledgements** The authors thank Prof. Zhiyu Li (China Pharmaceutical University, Nanjing, China) for kindly providing oroxylin A. The authors appreciate Jie Zhao, who works in the Animal

Experimental Center of Public Experimental Platform, for technical assistance.

**Author contributions** Jing Xia, Tingting Zhang, Ying Sun, Zhu Huang, and Guiying Yao performed biochemical and molecular biology experiments. Zhu Huang, Dingfang Shi, Dongshen Qin, Xuejun Yang, and Hao Liu performed neural damage assessment and behavioral experiments. Jing Xia, Tingting Zhang, Ying Sun, and Zhu Huang conducted formal analysis and data visualization. Jing Xia, Libin Wei, and Yongjian Guo constructed plasmids or provided essential reagents. Xiaoi Chang, Jun Gao, and Yongjian Guo provided technical support, discussions, and suggestions. Xiao-Yu Hou conceived and designed this project. Jing Xia, Ying Sun, and Xiao-Yu Hou wrote the original draft. Jun Gao and Xiao-Yu Hou reviewed and edited the manuscript. All authors have approved the final version of this manuscript.

**Funding** This study was supported by grants from the National Natural Science Foundation of China (No. 82173801 and 81673418 to Xiao-Yu Hou).

**Data availability** All data are available from the corresponding authors upon reasonable request.

## Declarations

**Ethical approval** No human samples were used in this study.

**Consent for publication** All authors have agreed for publication.

**Conflict of interest** All other authors declare no conflicts of interests.

**Open Access** This article is licensed under a Creative Commons Attribution-NonCommercial-NoDerivatives 4.0 International License, which permits any non-commercial use, sharing, distribution and reproduction in any medium or format, as long as you give appropriate credit to the original author(s) and the source, provide a link to the Creative Commons licence, and indicate if you modified the licensed material. You do not have permission under this licence to share adapted material derived from this article or parts of it. The images or other third party material in this article are included in the article's Creative Commons licence, unless indicated otherwise in a credit line to the material. If material is not included in the article's Creative Commons licence and your intended use is not permitted by statutory regulation or exceeds the permitted use, you will need to obtain permission directly from the copyright holder. To view a copy of this licence, visit <http://creativecommons.org/licenses/by-nc-nd/4.0/>.

## References

1. GBD 2019 Stroke Collaborators (2021) Global, regional, and national burden of stroke and its risk factors, 1990–2019: a systematic analysis for the global burden of disease study 2019. *Lancet Neurol* 20(10):795–820. [https://doi.org/10.1016/s1474-4422\(21\)00252-0](https://doi.org/10.1016/s1474-4422(21)00252-0)
2. Pu L, Wang L, Zhang R, Zhao T, Jiang Y, Han L (2023) Projected global trends in ischemic stroke incidence, deaths and disability-adjusted life years from 2020 to 2030. *Stroke* 54(5):1330–1339. <https://doi.org/10.1161/strokeaha.122.040073>
3. Thomalla G, Simonsen CZ, Boutitie F, Andersen G, Berthezene Y, Cheng B, Cheripelli B, Cho TH, Fazekas F, Fiehler J et al (2018) MRI-guided thrombolysis for stroke with unknown time of onset. *N Engl J Med* 379(7):611–622. <https://doi.org/10.1056/NEJMoa1804355>
4. Wang Y, Wu X, Zhu C, Mossa-Basha M, Malhotra A (2021) Bridging thrombolysis achieved better outcomes than direct thrombectomy after large vessel occlusion: an updated meta-analysis. *Stroke* 52(1):356–365. <https://doi.org/10.1161/strokeaha.120.031477>
5. Kim JS, Lee EJ, Chang DI, Park JH, Ahn SH, Cha JK, Heo JH, Sohn SI, Lee BC, Kim DE et al (2017) Efficacy of early administration of escitalopram on depressive and emotional symptoms and neurological dysfunction after stroke: a multicentre, double-blind, randomised, placebo-controlled study. *Lancet Psychiatry* 4(1):33–41. [https://doi.org/10.1016/s2215-0366\(16\)30417-5](https://doi.org/10.1016/s2215-0366(16)30417-5)
6. Rost NS, Brodtmann A, Pase MP, van Veluw SJ, Biffi A, Duering M, Hinman JD, Dichgans M (2022) Post-stroke cognitive impairment and dementia. *Circ Res* 130(8):1252–1271. <https://doi.org/10.1161/circresaha.122.319951>
7. Frank D, Gruenbaum BF, Zlotnik A, Semyonov M, Frenkel A, Boyko M (2022) Pathophysiology and current drug treatments for post-stroke depression: a review. *Int J Mol Sci* 23(23):15114. <https://doi.org/10.3390/ijms232315114>
8. Rangaraju V, Calloway N, Ryan TA (2014) Activity-driven local ATP synthesis is required for synaptic function. *Cell* 156(4):825–835. <https://doi.org/10.1016/j.cell.2013.12.042>
9. Magistretti PJ, Allaman I (2015) A cellular perspective on brain energy metabolism and functional imaging. *Neuron* 86(4):883–901. <https://doi.org/10.1016/j.neuron.2015.03.035>
10. Pulido C, Ryan TA (2021) Synaptic vesicle pools are a major hidden resting metabolic burden of nerve terminals. *Sci Adv* 7(49):eabi9027. <https://doi.org/10.1126/sciadv.abi9027>
11. Mengesdorf T, Jensen PH, Mies G, Aufenberg C, Paschen W (2002) Down-regulation of parkin protein in transient focal cerebral ischemia: a link between stroke and degenerative disease? *Proc Natl Acad Sci U S A* 99(23):15042–15047. <https://doi.org/10.1073/pnas.232588799>
12. Yao GY, Zhu Q, Xia J, Chen FJ, Huang M, Liu J, Zhou TT, Wei JF, Cui GY, Zheng KY et al (2018) Ischemic postconditioning confers cerebroprotection by stabilizing VDACs after brain ischemia. *Cell Death Dis* 9(10):1033. <https://doi.org/10.1038/s41419-018-1089-5>
13. Zhang T, Xu D, Trefts E, Lv M, Inuzuka H, Song G, Liu M, Lu J, Liu J, Chu C et al (2023) Metabolic orchestration of cell death by AMPK-mediated phosphorylation of RIPK1. *Science* 380(6652):1372–1380. <https://doi.org/10.1126/science.abn1725>
14. Jones TA (2017) Motor compensation and its effects on neural reorganization after stroke. *Nat Rev Neurosci* 18(5):267–280. <https://doi.org/10.1038/nrn.2017.26>
15. Douven E, Staals J, Freeze WM, Schievink SH, Hellebrekers DM, Wolz R, Jansen JF, van Oostenbrugge RJ, Verhey FR, Aalten P et al (2020) Imaging markers associated with the development of post-stroke depression and apathy: results of the cognition and affect after stroke—a prospective evaluation of risks study. *Eur Stroke J* 5(1):78–84. <https://doi.org/10.1177/2396987319883445>
16. Harper DG, Jensen JE, Ravichandran C, Perlis RH, Fava M, Renshaw PF, Iosifescu DV (2017) Tissue type-specific bioenergetic abnormalities in adults with major depression. *Neuropsychopharmacology* 42(4):876–885. <https://doi.org/10.1038/npp.2016.180>
17. Daws RE, Timmermann C, Giribaldi B, Sexton JD, Wall MB, Erritzoe D, Roseman L, Nutt D, Carhart-Harris R (2022) Increased global integration in the brain after psilocybin therapy for depression. *Nat Med* 28(4):844–851. <https://doi.org/10.1038/s41591-022-01744-z>
18. Gomez-Sanchez JC, Delgado-Esteban M, Rodriguez-Hernandez I, Sobrino T, Perez de la Ossa N, Reverte S, Bolaños JP, Gonzalez-Sarmiento R, Castillo J, Almeida A (2011) The human Tp53 Arg72Pro polymorphism explains different functional prognosis

- in stroke. *J Exp Med* 208(3):429–437. <https://doi.org/10.1084/jem.20101523>
19. Rodríguez C, Sobrino T, Agulla J, Bobo-Jiménez V, Ramos-Araque ME, Duarte JJ, Gómez-Sánchez JC, Bolaños JP, Castillo J, Almeida Á (2017) Neovascularization and functional recovery after intracerebral hemorrhage is conditioned by the Tp53 Arg72Pro single-nucleotide polymorphism. *Cell Death Differ* 24(1):144–154. <https://doi.org/10.1038/cdd.2016.109>
  20. Maor-Nof M, Shipony Z, Lopez-Gonzalez R, Nakayama L, Zhang YJ, Couthouis J, Blum JA, Castruita PA, Linares GR, Ruan K et al (2021) p53 is a central regulator driving neurodegeneration caused by C9orf72 poly(PR). *Cell* 184(3):689–708e20. <https://doi.org/10.1016/j.cell.2020.12.025>
  21. Almeida A, Sánchez-Morán I, Rodríguez C (2021) Mitochondrial-nuclear p53 trafficking controls neuronal susceptibility in stroke. *IUBMB Life* 73(3):582–591. <https://doi.org/10.1002/iub.2453>
  22. Brady CA, Jiang D, Mello SS, Johnson TM, Jarvis LA, Kozak MM, Kenzelmann Broz D, Basak S, Park EJ, McLaughlin ME et al (2011) Distinct p53 transcriptional programs dictate acute DNA-damage responses and tumor suppression. *Cell* 145(4):571–583. <https://doi.org/10.1016/j.cell.2011.03.035>
  23. Yoon KW, Byun S, Kwon E, Hwang SY, Chu K, Hiraki M, Jo SH, Weins A, Hakroush S, Cebulla A et al (2015) Control of signaling-mediated clearance of apoptotic cells by the tumor suppressor p53. *Science* 349(6247):1261669. <https://doi.org/10.1126/science.1261669>
  24. Boutelle AM, Attardi LD (2021) p53 and tumor suppression: it takes a network. *Trends Cell Biol* 31(4):298–310. <https://doi.org/10.1016/j.tcb.2020.12.011>
  25. Ho CJ, Lin RW, Zhu WH, Wen TK, Hu CJ, Lee YL, Hung TI, Wang C (2019) Transcription-independent and -dependent p53-mediated apoptosis in response to genotoxic and non-genotoxic stress. *Cell Death Discov* 5:131. <https://doi.org/10.1038/s41420-019-0211-5>
  26. Haapaniemi E, Botla S, Persson J, Schmierer B, Taipale J (2018) CRISPR-Cas9 genome editing induces a p53-mediated DNA damage response. *Nat Med* 24(7):927–930. <https://doi.org/10.1038/s41591-018-0049-z>
  27. Wang YH, Ho TLF, Hariharan A, Goh HC, Wong YL, Verkaik NS, Lee MY, Tam WL, van Gent DC, Venkiteswaran AR et al (2022) Rapid recruitment of p53 to DNA damage sites directs DNA repair choice and integrity. *Proc Natl Acad Sci U S A* 119(10):e2113233119. <https://doi.org/10.1073/pnas.2113233119>
  28. Mergenthaler P, Lindauer U, Dienel GA, Meisel A (2013) Sugar for the brain: the role of glucose in physiological and pathological brain function. *Trends Neurosci* 36(10):587–597. <https://doi.org/10.1016/j.tins.2013.07.001>
  29. Wei Y, Miao Q, Zhang Q, Mao S, Li M, Xu X, Xia X, Wei K, Fan Y, Zheng X et al (2023) Aerobic glycolysis is the predominant means of glucose metabolism in neuronal somata, which protects against oxidative damage. *Nat Neurosci* 26(12):2081–2089. <https://doi.org/10.1038/s41593-023-01476-4>
  30. Radhakrishnan SK, Gartel AL (2006) CDK9 phosphorylates p53 on serine residues 33, 315 and 392. *Cell Cycle* 5(5):519–521. <https://doi.org/10.4161/cc.5.5.2514>
  31. Yao JY, Xu S, Sun YN, Xu Y, Guo QL, Wei LB (2022) Novel CDK9 inhibitor oroxylin A promotes wild-type P53 stability and prevents hepatocellular carcinoma progression by disrupting both MDM2 and SIRT1 signaling. *Acta Pharmacol Sin* 43(4):1033–1045. <https://doi.org/10.1038/s41401-021-00708-2>
  32. Liu J, Zhang C, Hu W, Feng Z (2019) Tumor suppressor p53 and metabolism. *J Mol Cell Biol* 11(4):284–292. <https://doi.org/10.1093/jmcb/mjy070>
  33. Krstic J, Reinisch I, Schindlmaier K, Gallhuber M, Riahi Z, Berger N, Kupper N, Moyschewitz E, Auer M, Michenthaler H et al (2022) Fasting improves therapeutic response in hepatocellular carcinoma through p53-dependent metabolic synergism. *Sci Adv* 8(3):eabh2635. <https://doi.org/10.1126/sciadv.abh2635>
  34. Duplan E, Giordano C, Checler F, Alves da Costa C (2016) Direct  $\alpha$ -synuclein promoter transactivation by the tumor suppressor p53. *Mol Neurodegener* 11:13. <https://doi.org/10.1186/s13024-016-0079-2>
  35. Farmer KM, Ghag G, Puangmalai N, Montalbano M, Bhatt N, Kaye R (2020) P53 aggregation, interactions with tau, and impaired DNA damage response in Alzheimer's disease. *Acta Neuropathol Commun* 8(1):132. <https://doi.org/10.1186/s40478-020-01012-6>
  36. Rostovtseva T, Colombini M (1996) ATP flux is controlled by a voltage-gated channel from the mitochondrial outer membrane. *J Biol Chem* 271(45):28006–28008. <https://doi.org/10.1074/jbc.271.45.28006>
  37. Fang D, Maldonado EN (2018) VDAC regulation: a mitochondrial target to stop cell proliferation. *Adv Cancer Res* 138:41–69. <https://doi.org/10.1016/bs.acr.2018.02.002>
  38. Herrero-Mendez A, Almeida A, Fernández E, Maestre C, Moncada S, Bolaños JP (2009) The bioenergetic and antioxidant status of neurons is controlled by continuous degradation of a key glycolytic enzyme by APC/C-Cdh1. *Nat Cell Biol* 11(6):747–752. <https://doi.org/10.1038/ncb1881>
  39. Geisler S, Holmström KM, Skujat D, Fiesel FC, Rothfuss OC, Kahle PJ, Springer W (2010) PINK1/Parkin-mediated mitophagy is dependent on VDAC1 and p62/SQSTM1. *Nat Cell Biol* 12(2):119–131. <https://doi.org/10.1038/ncb2012>
  40. Li J, Lu J, Mi Y, Shi Z, Chen C, Riley J, Zhou C (2014) Voltage-dependent anion channels (VDACs) promote mitophagy to protect neuron from death in an early brain injury following a subarachnoid hemorrhage in rats. *Brain Res* 1573:74–83. <https://doi.org/10.1016/j.brainres.2014.05.021>
  41. Ham SJ, Lee D, Yoo H, Jun K, Shin H, Chung J (2020) Decision between mitophagy and apoptosis by Parkin via VDAC1 ubiquitination. *Proc Natl Acad Sci U S A* 117(8):4281–4291. <https://doi.org/10.1073/pnas.1909814117>
  42. Di Y, He YL, Zhao T, Huang X, Wu KW, Liu SH, Zhao YQ, Fan M, Wu LY, Zhu LL (2015) Methylene blue reduces acute cerebral ischemic injury via the induction of mitophagy. *Mol Med* 21(1):420–429. <https://doi.org/10.2119/molmed.2015.00038>
  43. Mao Z, Tian L, Liu J, Wu Q, Wang N, Wang G, Wang Y, Seto S (2022) Ligustilide ameliorates hippocampal neuronal injury after cerebral ischemia reperfusion through activating PINK1/Parkin-dependent mitophagy. *Phytomedicine* 101:154111. <https://doi.org/10.1016/j.phymed.2022.154111>
  44. Dambal S, Shah M, Mihelich B, Nonn L (2015) The microRNA-183 cluster: the family that plays together stays together. *Nucleic Acids Res* 43(15):7173–7188. <https://doi.org/10.1093/nar/gkv703>
  45. Xu S, Witmer PD, Lumayag S, Kovacs B, Valle D (2007) MicroRNA (miRNA) transcriptome of mouse retina and identification of a sensory organ-specific miRNA cluster. *J Biol Chem* 282(34):25053–25066. <https://doi.org/10.1074/jbc.M700501200>
  46. Griggs EM, Young EJ, Rumbaugh G, Miller CA (2013) MicroRNA-182 regulates amygdala-dependent memory formation. *J Neurosci* 33(4):1734–1740. <https://doi.org/10.1523/jneurosci.2873-12.2013>
  47. Woldemichael BT, Jawaid A, Kremer EA, Gaur N, Krol J, Marchais A, Mansuy IM (2016) The microRNA cluster miR-183/96/182 contributes to long-term memory in a protein phosphatase 1-dependent manner. *Nat Commun* 7:12594. <https://doi.org/10.1038/ncomms12594>
  48. Zhou L, Miller C, Miraglia LJ, Romero A, Mure LS, Panda S, Kay SA (2021) A genome-wide microRNA screen identifies the microRNA-183/96/182 cluster as a modulator of circadian

- rhythms. *Proc Natl Acad Sci U S A* 118(1):e2020454118. <https://doi.org/10.1073/pnas.2020454118>
49. Tang Y, Yang J, Ye C, Xu X, Cai M, Zhang Y, Lu H, Mo F, Li H, Shen H (2022) miR-182 mediated the inhibitory effects of NF- $\kappa$ B on the GPR39/CREB/BDNF pathway in the hippocampus of mice with depressive-like behaviors. *Behav Brain Res* 418:113647. <https://doi.org/10.1016/j.bbr.2021.113647>
  50. Alhadidi QM, Xu L, Sun X, Althobaiti YS, Almalki A, Alsaab HO, Sary CM (2022) MiR-182 inhibition protects against experimental stroke in vivo and mitigates astrocyte injury and inflammation in vitro via modulation of cortactin activity. *Neurochem Res* 47(12):3682–3696. <https://doi.org/10.1007/s11064-022-03718-6>
  51. Zhu L, Zhou X, Li S, Liu J, Yang J, Fan X, Zhou S (2020) miR-183-5p attenuates cerebral ischemia injury by negatively regulating PTEN. *Mol Med Rep* 22(5):3944–3954. <https://doi.org/10.3892/mmr.2020.11493>
  52. Wu Q, Wu JH, Ye ZY, She W, Peng WJ, Zhang HX, Qi C, Tian T, Hou XY, Gao J (2024) Exosomes from hypoxia-treated mesenchymal stem cells: promoting neuroprotection in ischemic stroke through miR-214-3p/PTEN mechanism. *Mol Neurobiol*. <https://doi.org/10.1007/s12035-024-04056-0>
  53. Guo S, Li ZZ, Gong J, Xiang M, Zhang P, Zhao GN, Li M, Zheng A, Zhu X, Lei H et al (2015) Oncostatin M confers neuroprotection against ischemic stroke. *J Neurosci* 35(34):12047–12062. <https://doi.org/10.1523/jneurosci.1800-15.2015>
  54. Gao JX, Li Y, Wang SN, Chen XC, Lin LL, Zhang H (2019) Overexpression of microRNA-183 promotes apoptosis of substantia nigra neurons via the inhibition of OSMR in a mouse model of Parkinson's disease. *Int J Mol Med* 43(1):209–220. <https://doi.org/10.3892/ijmm.2018.3982>
  55. Xu J, Xu S, Fang Y, Chen T, Xie X, Lu W (2019) Cyclin-dependent kinase 9 promotes cervical cancer development via AKT2/p53 pathway. *IUBMB Life* 71(3):347–356. <https://doi.org/10.1002/iub.1983>
  56. Fong SY, Wong YC, Zuo Z (2014) Development of a SPE-LC/MS/MS method for simultaneous quantification of baicalin, wogonin, oroxylin A and their glucuronides baicalin, wogonoside and oroxyloside in rats and its application to brain uptake and plasma pharmacokinetic studies. *J Pharm Biomed Anal* 97:9–23. <https://doi.org/10.1016/j.jpba.2014.03.033>
  57. Lu L, Guo Q, Zhao L (2016) Overview of oroxylin A: a promising flavonoid compound. *Phytother Res* 30(11):1765–1774. <https://doi.org/10.1002/ptr.5694>
  58. Sajeev A, Hegde M, Girisa S, Devanarayanan TN, Alqahtani MS, Abbas M, Sil SK, Sethi G, Chen JT, Kunnumakkara AB (2022) Oroxylin A: a promising flavonoid for prevention and treatment of chronic diseases. *Biomolecules* 12(9):1185. <https://doi.org/10.3390/biom12091185>
  59. Kim DH, Jeon SJ, Son KH, Jung JW, Lee S, Yoon BH, Choi JW, Cheong JH, Ko KH, Ryu JH (2006) Effect of the flavonoid, oroxylin A, on transient cerebral hypoperfusion-induced memory impairment in mice. *Pharmacol Biochem Behav* 85(3):658–668. <https://doi.org/10.1016/j.pbb.2006.10.025>
  60. Chien JY, Lin SF, Chou YY, Huang CF, Huang SP (2021) Protective effects of oroxylin A on retinal ganglion cells in experimental model of anterior ischemic optic neuropathy. *Antioxid (Basel)* 10(6):902. <https://doi.org/10.3390/antiox10060902>

**Publisher's note** Springer Nature remains neutral with regard to jurisdictional claims in published maps and institutional affiliations.